Broadband dielectric spectroscopy of water confined in MCM-41 molecular sieve materials—low-temperature freezing phenomena

2005 J. Phys.: Condens. Matter 17 2843

(http://iopscience.iop.org/0953-8984/17/19/003)

INSTITUTE OF PHYSICS PUBLISHING JOURNAL OF PHYSICS: CONDENSED MATTER

J. Phys.: Condens. Matter **17** (2005) 2843–2857 doi:10.1088/0953-8984/17/19/003

Broadband dielectric spectroscopy of water confined in MCM-41 molecular sieve materials—low-temperature freezing phenomena

Juras Banys[1], Martynas Kinka[1], Jan Macutkevic[1], Georg Völkel[2], Winfried Böhlmann[2], Venkatesan Umamaheswari[2], Martin Hartmann[3] and Andreas Pöppl[2]

[1] Faculty of Physics, Vilnius University, Sauletekio 9, 10222 Vilnius, Lithuania
[2] University of Leipzig, Faculty of Physics and Geoscience, Linnéstraße 5, D-04103 Leipzig, Germany
[3] Department of Chemistry, Chemical Technology, University of Kaiserslautern, Erwin-Schrödinger-Straße 54, D-67663 Kaiserslautern, Germany

Received 1 February 2005, in final form 16 March 2005
Published 29 April 2005
Online at stacks.iop.org/JPhysCM/17/2843

Abstract

Dielectric properties of water adsorbed in pure siliceous and aluminium containing mesoporous MCM-41 materials have been investigated in the frequency range from 20 Hz to 1 MHz. The dielectric spectra revealed three dispersion regions, liquid-like free water in the centre of the mesopores, an intermediate water layer with reduced mobility, and an interfacial water layer at the inner surface of the mesopores. The analysis of the relaxation time distribution by means of a double-well potential indicates a strong dependence of the barrier height of reorienting water molecules dipoles in the interfacial layer on the Si/Al ratio in the framework.

M Supplementary data files are available from stacks.iop.org/JPhysCM/17/2843

1. Introduction

Since their discovery more than one decade ago, mesoporous MCM-41 molecular sieve materials [1] have triggered widespread interest in many research fields [2] because of their unique structural and chemical properties. This class of silica tube-like materials features extremely large specific surface areas exceeding 1000 $m^2\ g^{-1}$. The molecular sieves possess uniformly sized mesopores whose diameter can be controlled between 1.5 and 8 nm by the synthesis conditions chosen and template used. Whereas the mesopores of MCM-41 are arranged in a regular hexagonal array, the silicon dioxide forming the walls around these tubes shows an amorphous structure [3]. The silicon can be partially substituted by various metal ions [2] in order to modify the chemical properties of the inner surface of the molecular sieve materials. Most commonly trivalent aluminium is used for framework incorporation,

which results in a net negative charge of the framework of such AlMCM-41 materials. The negative charge is either compensated by cations at extra framework sites or by the formation of Brønsted acid sites (SiOHAl groups) in the walls of the mesopores, which are moderately acidic [4]. Alternatively, the relatively large pore size allows the fixation of catalytically active complexes [2, 5] and metal clusters [2, 6] at the surface of the mesopores. Thus, MCM-41 materials have especially attracted interest in adsorptive and catalytic applications involving large molecules [2]. Other promising applications are the use of MCM-41 materials as hosts for semiconducting [7–11] and ferroelectric [12] nanomaterials as well as for the study of confined liquids [13–17] and polymers [17, 18].

Many of the envisaged applications involve aqueous phases at one or the other step. Therefore information about the structure, dynamics, and freezing phenomena of water confined in the mesopores is of uttermost importance to control and optimize catalytic activity or pore fillings by guest molecules. The physical properties of water adsorbed in mesoporous MCM-41 materials with different pore sizes have been studied by ^{1}H nuclear magnetic resonance (NMR) [16], x-ray powder diffraction (XRD) [15, 19], neutron scattering [20–22], and isothermal adsorption [14] experiments. In general two types of water were found: one water phase displays the typical freezing behaviour of a confined liquid into a cubic ice structure whereas the second phase of more strongly bound water undergoes a gradually freezing in a glass-type manner at lower temperatures. Naturally the two phases have been assigned to free water molecules in the centre of the mesopores and an interfacial water layer between the free water and the solid surface of the pores.

Studies of water confined in various other silica based pores showed different structural and dynamical properties of confined water compared to the bulk. A depression of the freezing point was always observed along with the freezing–melting hysteresis [23]. The shift of the freezing temperature shows good agreement with the Gibbs–Thomson equation for pores larger than 5 nm and quite big deviations were observed for smaller pores [33]. NMR and x-ray diffraction studies revealed several types of water inside pores. 'Bound' water—a few disordered water molecule layers near the pore walls with a structure that is different from that of the bulk ice and free liquid, relatively free water in the centre of the mesopores and an intermediate layer between these two [34]. It was found that water in the centres of mesopores freezes rather to a cubic ice I_c instead of an ordinary hexagonal phase I_h [15]. This phenomenon is also very dependent on the pore size. It was found that the confined fluid freezes into a single-crystalline structure for average pore diameters greater than 20σ, where σ is the diameter of the fluid molecule. For average pore sizes between 20 and 15σ, part of the confined fluid freezes into a frustrated crystal structure with the rest forming an amorphous region. For pore sizes smaller than 15σ, even partial crystallization did not occur [23].

Comparable results have been obtained by dielectric spectroscopy for nitrobenzene-loaded MCM-41 [23] and water confined in the three-dimensional, cubic pore system of MCM-48 [24]. Some authors stressed that the characterization of the interfacial water layer seems to be of particular interest because such studies are expected to provide new insight into the interaction between the fluid and solid surface [23, 24], the influence of the interfacial water on the phase transition between free water and the ice phase [19] and supercooling phenomena of confined water [15].

In this work we investigate the dynamics of water confined in the mesopores of pure siliceous MCM-41 in comparison with AlMCM-41 materials with two different n_{Si}/n_{Al} framework ratios by broadband dielectric spectroscopy in the temperature range 100 K $\leqslant T \leqslant$ 400 K. The study focuses on the freezing behaviour of the interfacial water layer between the free water in the centre of the mesopores and the pore walls. On the basis of a regularization procedure [25] the actual distribution of the relaxation times of the water molecules in the

interfacial layer is directly evaluated from the measured frequency dependences of the real and imaginary parts of the dielectric constant ε^* at various temperatures. We have to note that this approach is model independent and now an *a priori* model for the distribution function of the relaxation times has to be assumed in advance. Later these actual relaxation time distributions are interpreted in terms of a physical model. In a first approximation, we employ an asymmetric double-minimum potential [26, 27] for the water dipole moments to model the interaction of the water molecules in the interfacial layer at the walls of the mesopores in MCM-41 and AlMCM-41 materials.

2. Experimental section

2.1. Sample preparation

AlMCM-41 materials with n_{Si}/n_{Al} ratios of 64 (sample AlMCM-41(a)) and 16 (sample AlMCM-41(b)) were synthesized according to the following procedure. Aluminium sulfate (Aldrich) was added to an aqueous solution of cetyltrimethylammoniumbromide (CTAB; Aldrich, 25 wt%) and stirred for 1 h. Then Aerosil 200 (Degussa) was added in small amounts to the solution and thereafter a suspension of sodium water glass (Aldrich) dissolved in water was added. The molar composition of the resulting gels was 0.009 $Al_2(SO_4)_3$:1 SiO_2:0.31 CTAB:0.41 Na_2O:31.27 H_2O (n_{Si}/n_{Al} ratio of 64, sample AlMCM-41(a)) and 0.036 Al_2 (SO_4):1 SiO_2:0.38 CTAB:0.41 Na_2O:31.27 H_2O (n_{Si}/n_{Al} ratio of 16, sample AlMCM-41(b)). Finally, the gel was stirred for 1 h, transferred into a polypropylene bottle and placed in a preheated oven. After heating the starting gel at 90 °C for 24 h, the polypropylene bottle was cooled to a comfortable handling temperature, opened and a titration was performed with 1 N sulfuric acid to adjust the pH to 10. This procedure was repeated after 48 and 72 h. After a reaction time of 96 h the pH value was measured again and found to be around 10. The pure siliceous MCM-41 material (sample MCM-41) was synthesized in a similar way, adding to an aqueous solution of CTAB the silicon source and then the suspension of sodium water glass. This gel was vigorously stirred for 1 h and hydrothermally treated at 90 °C for 96 h. The obtained solid products were filtered off and washed first with distilled water and in a second step with methanol to remove the residual template. After drying the solid product at 90 °C for 8 h in air, it was calcined for 12 h at 540 °C. All samples were characterized by nitrogen adsorption–desorption at 77 K, XRD powder diffraction, and ^{27}Al- and ^{29}Si magic angle spinning (MAS) NMR spectroscopy. The mesoporous materials were carefully compacted to disc-shaped pellets (20, 0.5 mm thickness) to avoid structural collapse. Later the samples were stored at ambient atmosphere to allow for water adsorption in the mesopores.

2.2. Dielectric measurements

The complex permittivity $\varepsilon^* = \varepsilon' - i\varepsilon''$ was measured by a capacitance bridge HP4284A in the frequency range 20 Hz–1 MHz. The disc-shaped sample was placed in the coaxial line between the inner conductor and short end, which were freshly polished for each measurement for better electrical contact. Measurements have been performed on cooling and heating at a rate of about 0.25 K min^{-1}. Each measurement started from cooling, and after reaching 110 K the sample was heated up to 420 K. We must remark that after several temperature cycles the results were fully reproducible and identical for the same sample.

Table 1. Characterization data of calcined samples MCM-41, AlMCM-41(a), and AlMCM-41(b).

Sample	d_{100} (nm)	V_p (ml g^{-1})	S_{BET} (m^2 g^{-1})	d_p (nm)
MCM-41	3.744	1.00	894	0.37
AlMCM-41(a)	4.184	0.90	879	0.38
AlMCM-41(b)	3.941	1.47	997	0.38

3. Results and discussion

3.1. Sample characterization

Before dielectric measurements the quality of the calcined samples MCM-41, AlMCM-41(a), and AlMCM-41(b) was checked by XRD powder diffraction, nitrogen adsorption–desorption measurements, and ^{27}Al- and ^{29}Si MAS NMR spectroscopy. XRD powder diffractograms of all three samples showed the four typical low-angle peaks of MCM-41 type materials which are indexed according to a hexagonal unit cell [1–3]. The corresponding spacing values d_{100} together with the pore volumes V_p and the BET surface areas S_{BET} as determined by the N_2 adsorption–desorption studies are summarized in table 1. All the three materials display high BET surface area confirming their mesoporosity; the adsorption isotherms obtained for these materials are also characteristic of mesoporous materials with uniform pore size. The pore size distributions were calculated from the N_2 adsorption–desorption data assuming a cylindrical pore geometry. The mean pore diameters d_p were determined from the maximum of the narrow pore size distributions and are likewise summarized in table 1. ^{27}Al MAS NMR spectra of samples AlMCM-41(a) and AlMCM-41(b) displayed a strong peak of tetrahedrally coordinated aluminium at about 55 ppm, confirming aluminium incorporation on framework sites. Furthermore, the ^{29}Si MAS NMR studies revealed that the aluminium is incorporated into the structure of mesoporous material which is shown by an intense peak at about -105 ppm assigned to Si(3Si, 1Al sites). XRD powder diffractograms, nitrogen adsorption isotherms, and calculated pore size distributions are given in the supplementary section (supplementary information available at stacks.iop.org/JPhysCM/17/2843).

3.2. Overall dielectric relaxation of water in MCM-41 type materials

The dielectric response of water confined in mesoporous MCM-41 molecular sieve materials shows a rich variety of different water phases with characteristic dynamics. Figure 1 illustrates the temperature dependence of the real and imaginary parts of permittivity between 100 and 400 K of adsorbed water in the pure siliceous MCM-41 sample at different frequencies. There are three dispersion regions of the adsorbed water molecules (figure 1): (1) in the temperature range between 280 and 340 K, (2) in the range between 220 and 400 K and (3) at low temperatures between 120 and 220 K, as shown in the insets of figure 1. We must remark that no freezing–melting hysteresis was observed for the whole temperature range. On the basis of the observed three dispersion regions we tentatively classify the confined water molecules into three types according to their dynamics: (i) liquid-like free water, which is located in the centre of the pores, (ii) an intermediate water layer with reduced mobility between the free water in the centre of the mesopores and an interfacial layer at the pore surface, and (iii) immobilized water molecules in an interfacial layer at the inner surface of the pores. To verify this assignment we have performed the following experiment. In a first step, complex permittivity of the MCM-41 material has been measured in a heating cycle from 110 up to 500 K. The results are basically identical to those results presented in figure 1. Thereafter,

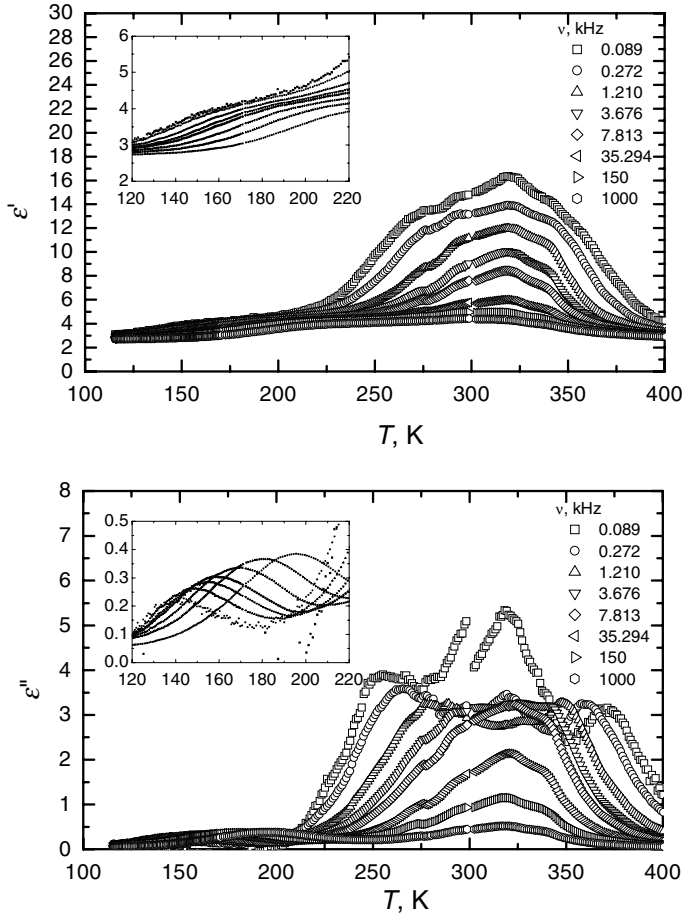

Figure 1. Temperature dependence of the real and imaginary parts of permittivity of sample MCM-41.

the sample was kept at 500 K for two hours to remove relatively weakly adsorbed water molecules. Then, the temperature dependence of the real and imaginary parts of permittivity of the sample was measured again on a cooling cycle down to 100 K. The obtained results are presented in figure 2. The relatively free unbound water of fraction (i), which was confined in the middle of the pores, is completely evaporated by the thermal treatment. Some water of the intermediate phase (ii) (dispersion in the temperature range 220–400 K) remains in the mesopores after the thermal treatment, but its dielectric response is strongly diminished. In contrast to the fractions (i) and (ii), the dispersion region (iii) at low temperatures, i.e. the temperature frequency dependence of the permittivity, has not changed after this moderate dehydration of MCM-41. Therefore, it seems to be justified to assign region (iii) to more strongly bound water molecules in an interfacial layer on the inner surface of the mesopores. A similar behaviour has been observed for ethylene and propylene glycol confined in porous glasses [17] where likewise three phases of the adsorbed molecules were observed.

Analogous temperature dependences of the real and imaginary parts of permittivity as observed for the pure siliceous MCM-41 material were found for the aluminium-containing samples AlMCM-41(a) (figure 3) and AlMCM-41(b) (figure 4). Again, we distinguish three

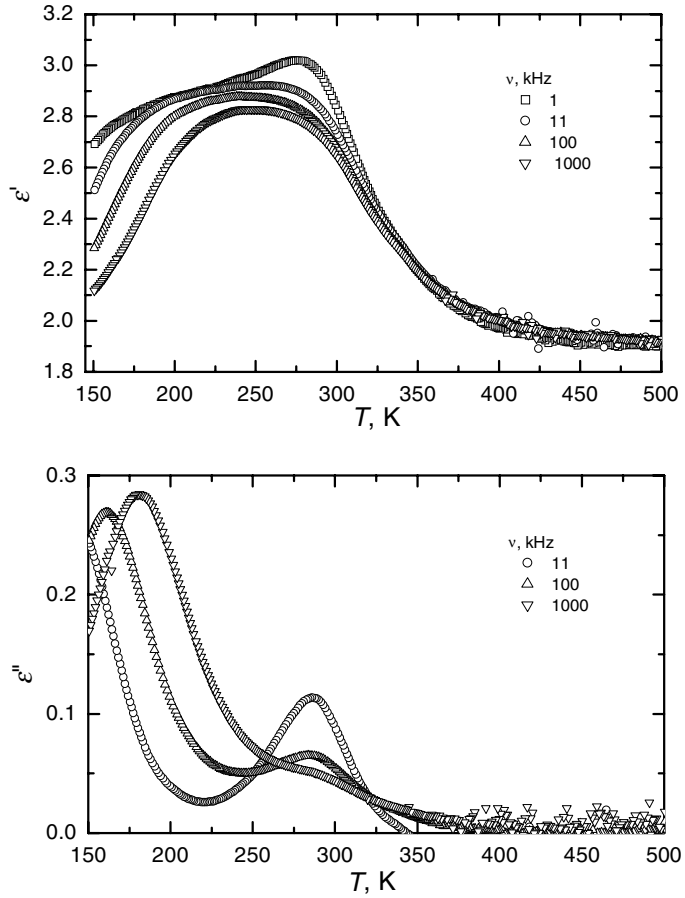

Figure 2. Temperature dependence of the real and imaginary parts of permittivity of sample MCM-41 after heating at 500 K for 2 h.

dispersion regions which are assigned in analogy to those found in the sample MCM-41 to (i) relatively free water in the centre of the mesopores, (ii) an intermediate water phase, and (iii) adsorbed water molecules forming an interfacial layer with the surface of the pores.

3.3. Dielectric relaxation of water in the interfacial layer in MCM-41 type materials

Most studies on water confined in MCM-41 [15, 16, 19–22] and MCM-48 [24] materials focus on the free water in the centre of the pores. Little is known about the structure and dynamics of the water in the interfacial layer with the pore walls. Therefore, we will focus on the low temperature dispersion range (iii) of that interfacial layer in this paper.

As shown in the insets of figures 1, 3, and 4 the temperature dependences of the real and imaginary parts of permittivity have similar shape compared with those of dipolar glasses [27–29]. Obtained frequency dependences, illustrated in figures 5–7 for selected temperatures, of complex permittivity are much broader as expected for a Debye-type dispersion with FWFM of 1.14 decades. This behaviour of ε'' does not allow a reliable estimation of the relaxation time using conventional relaxation models or empirical equations. Therefore, a special algorithm was developed to solve this problem [27].

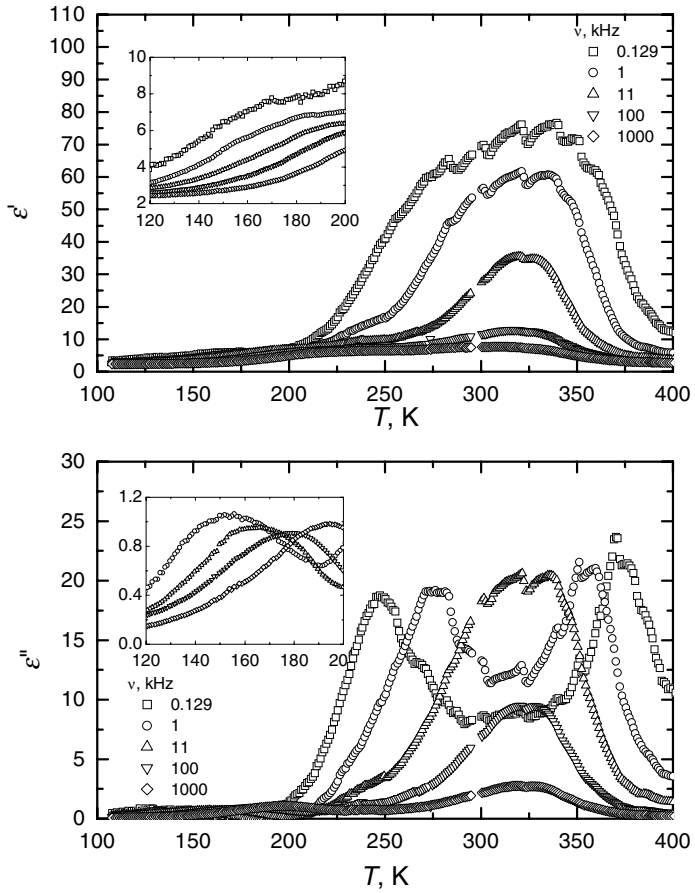

Figure 3. Temperature dependence of the real and imaginary parts of permittivity of sample AlMCM-41(a).

3.4. Analysis of the relaxation time distribution of water in the interfacial layer in MCM-41 type materials

The original program performs the direct calculation of the relaxation time distribution function $g(\tau)$ from the frequency dependence of the complex permittivity at fixed temperatures according to superposition of Debye-like processes

$$\varepsilon'(\nu) = \varepsilon_\infty + \int_0^\infty \frac{g(\tau)}{1+(2\pi\nu\tau)^2}\,\mathrm{d}(\ln\tau), \qquad \varepsilon''(\nu) = \int_0^\infty \frac{2\pi\nu\tau g(\tau)}{1+(2\pi\nu\tau)^2}\,\mathrm{d}(\ln\tau). \tag{1}$$

The high-frequency limiting value ε_∞ and the total contribution of the dipoles to the permittivity $\Delta\varepsilon = \int g\ (\tau)\,\mathrm{d}\ (\ln\tau)$ can be either given together with the initial data or defined during the solution. The basic integral transformations in equation (1) can be presented as the following linear matrix equation:

$$\boldsymbol{AX} = \boldsymbol{T}, \tag{2}$$

where the matrix $\boldsymbol{A}$ components are obtained by proper discretization of the integral transformation kernels and vectors $\boldsymbol{T}$ and $\boldsymbol{X}$ components correspond to discretized values of the permittivity (as initial data) and distribution of relaxation times (as the result), respectively.

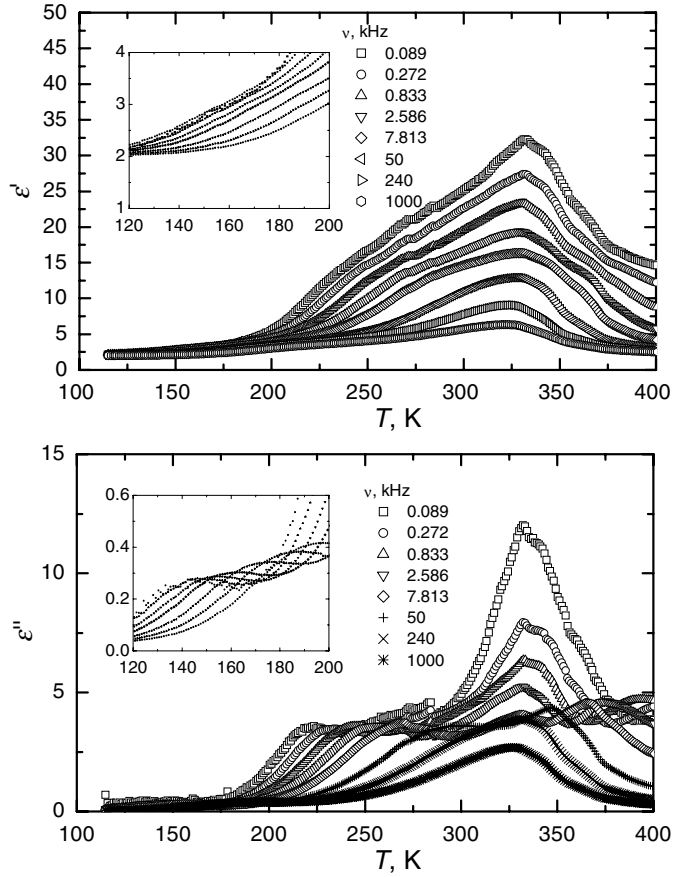

Figure 4. Temperature dependence of the real and imaginary parts of permittivity of sample AlMCM-41(b).

Equation (2) represents an ill posed problem and cannot be solved straightforwardly. It is, therefore, replaced by the following minimization problem:

$$\Phi = \|\boldsymbol{T} - \boldsymbol{AX}\| + \alpha\|\boldsymbol{RX}\|, \tag{3}$$

where α is the regularization parameter and $\boldsymbol{R}$ is the regularization matrix, which corresponds to the second derivative $g''(\tau)$. The exclusion of negative spectral components $g(\tau)$ is added as an additional constraint. This constrained regularized minimization problem is solved by the least squares technique employing the simplified version of the CONTIN program developed by Prowentcher [25].

The obtained relaxation time distributions of the water molecules in the interfacial layer are presented in figure 8 for MCM-41, AlMCM-41(a), and AlMCM-41(b).

So far, the calculation of the relaxation time distributions (figure 8) from the experimentally obtained frequency dependence of the permittivity has been performed independently of a specific physical model. In order to interpret the temperature dependence of the relaxation time distributions, a model for the reorientation of the electric dipole moments of the water molecules has to be assumed. It is generally accepted that the presence of orientational defects in the hydrogen bond system is the major cause for the dipolar relaxation in ice [31]. Suggested structures for such orientational defects are for instance OH $\cdots$ HO species (D defect) between

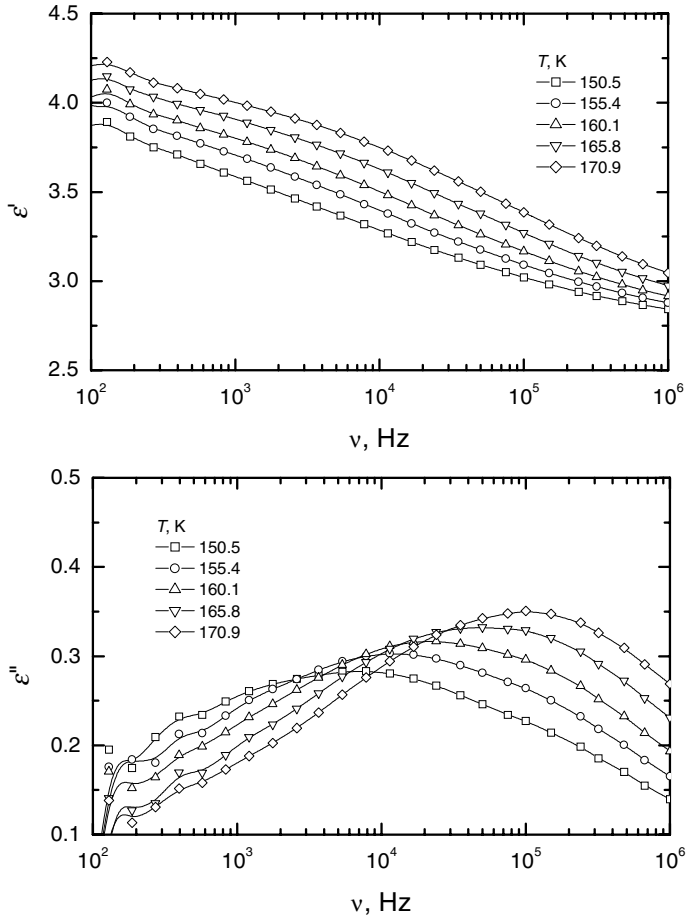

Figure 5. Frequency dependence of the real and imaginary parts of permittivity of MCM-41 material.

pairs of neighbouring OH groups or pairs of O · · · O atoms facing each other (L defect), which are not bound by hydrogen bonds [31, 32]. The defects migrate by 120° rotation of a water molecule at a defect site giving rise to the dielectric relaxation. We have to note that for water in the interfacial layer even more defects may be expected due to the interaction of the molecules with the solid surface. In the following, we will model the reorientation of the dipole moment of the water molecules in the interfacial layer by assuming that the water molecules are moving in a double-well potential where the interaction between the dipole moments is expressed in terms of an effective potential according to the mean field approximation. Then, the relaxation time of such a system is given by [26]

$$\tau = \tau_0 \frac{\exp[E_b/(T - T_0)]}{2\cosh(A/2k_B T)}, \tag{4}$$

where E_b is the barrier height, A the asymmetry of a double-well potential, T_0 the freezing temperature, and τ_0 is the relaxation time at $T \to \infty$. This equation is similar to the Vogel–Fulcher equation, except the denominator, which accounts for the asymmetry of the local potential produced by the mean field influence of all other dipoles. We further assume that both the asymmetry A and the potential barrier height E_b of the local potential are randomly

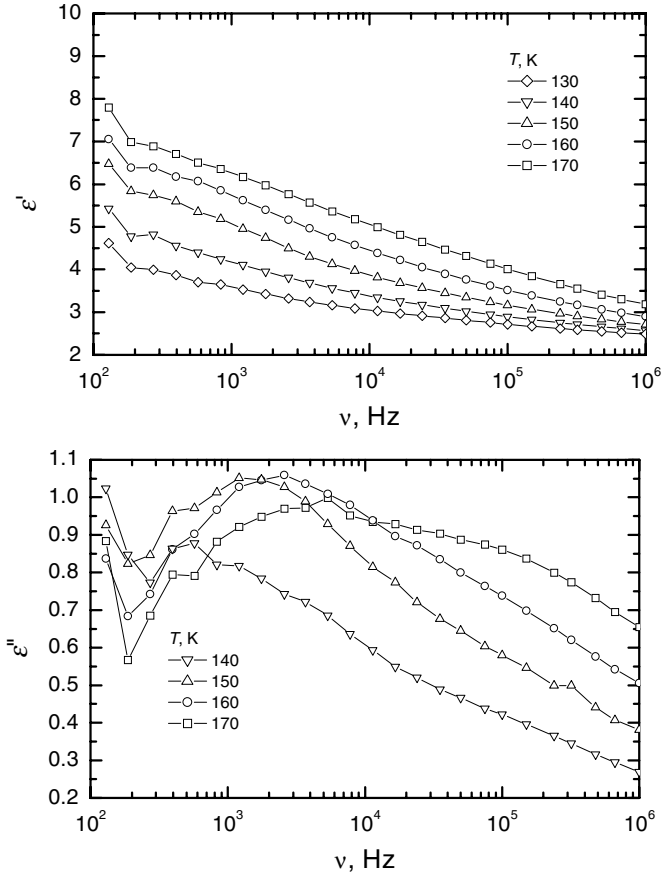

Figure 6. Frequency dependence of the real and imaginary parts of permittivity of sample AlMCM-41(a).

distributed around their mean values A_0 and E_{b0} according to the Gaussian law resulting in the distribution function

$$w(E_b) = \frac{1}{\sqrt{2\pi}\sigma_E} \exp\left(-\frac{(E_b - E_{b0})^2}{2\sigma_E^2}\right) \tag{5}$$

with

$$w(A) = \frac{1}{\sqrt{2\pi}\sigma_A} \exp\left(-\frac{(A - A_0)^2}{2\sigma_A^2}\right), \tag{6}$$

where σ_E and σ_A are the standard deviations of E_b and A, respectively, from their mean values. The distribution function of the relaxation times is then given by

$$w(\ln\tau) = \int_{-\infty}^{\infty} w(A) W[E_b(A,\tau)] \frac{\partial E_b}{\partial(\ln\tau)}\, dA, \tag{7}$$

where $E_b(A,\tau)$ is the dependence of E_b on A for a given τ, derived from equation (4). Fits with the experimentally obtained relaxation time distributions were performed simultaneously at ten different temperatures for all three samples. The obtained parameters τ_0, T_0, and A_0 are summarized in table 2. Spectra with the fits are presented in figure 8. From these fits the

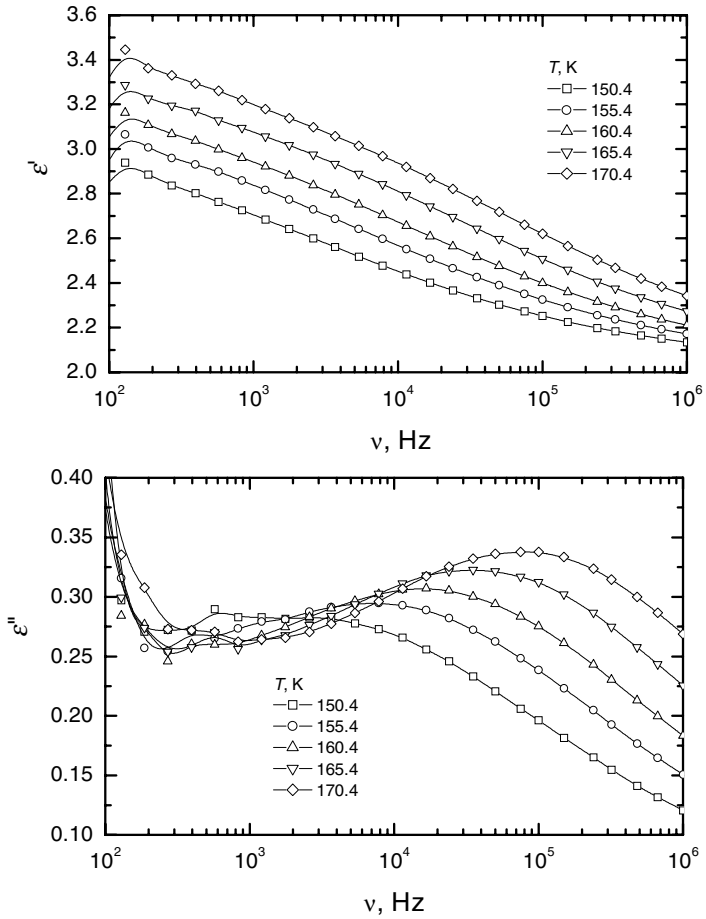

Figure 7. Frequency dependence of the real and imaginary parts of permittivity of sample AlMCM-41(b).

Table 2. Double-well parameters for samples MCM-41, AlMCM-41(a), and AlMCM-41(b).

Sample	τ_0 (s)	T_0 (K)	A_0 (kJ mol^{-1})
MCM-41	3579×10^{-15}	25.8	0
AlMCM-41(a)	4104×10^{-12}	21.4	0
AlMCM-41(b)	2631×10^{-10}	21.3	0

temperature dependence of the double-well parameters has been obtained, which is presented in figure 9. We have to note, however, that due to the different temperature regions where the main dispersion occurs the parameters are not defined at the same temperature.

Our analysis of the relaxation time distribution by means of the simple model of a double-well potential supports previous results obtained by XRD and neutron scattering [15, 19–22], where a glassy behaviour of the interfacial water layer has been predicted. The determined freezing temperatures of about $T_0 \approx$ 21–26 K (table 2) are typical for the glassy state of hydrogen-bonded systems as observed for a variety of different proton glasses such as mixed solid solutions of betaine phosphate–betaine phosphite (BP–BPI) mixed crystals [27].

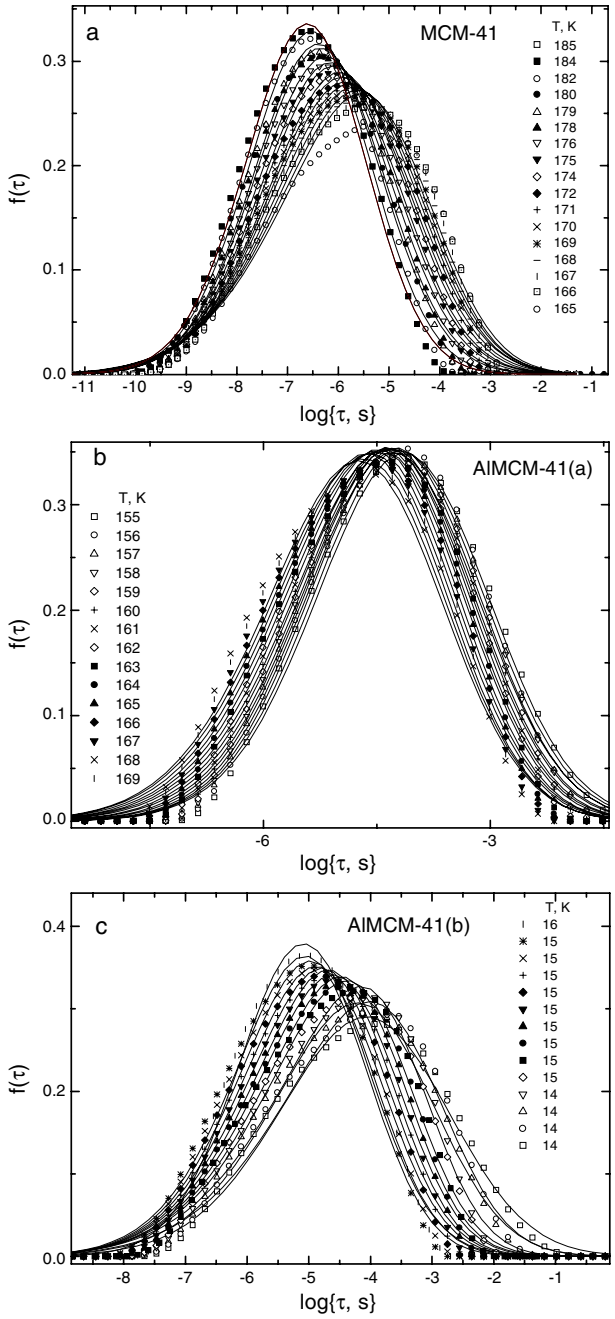

Figure 8. Temperature dependence of the relaxation time distribution of samples (a) MCM-41, (b) AlMCM-41(a), and (c) AlMCM-41(b). Lines are the best fits with equations (5)–(7).

Whereas the freezing temperatures do not differ significantly, the attempt relaxation times τ_0 increase with rising aluminium framework concentration (table 2). In a general approach to interpret the dielectric relaxation of confined water, Ryabov *et al* [30] developed the free

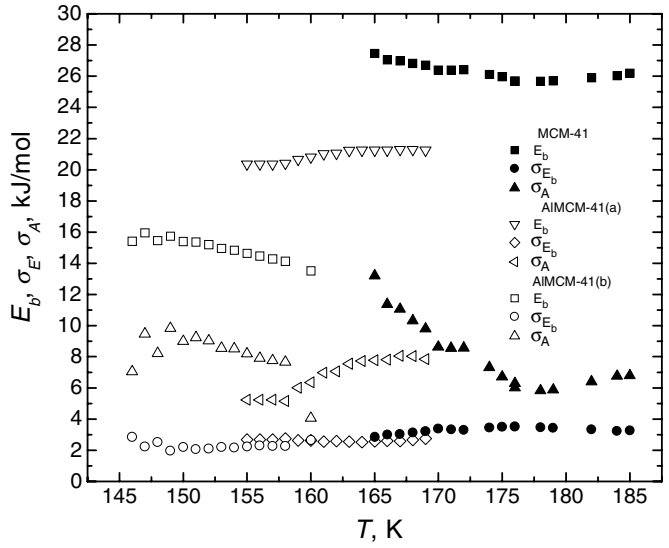

Figure 9. Temperature dependence of double-well potential parameters E_b, σ_E and σ_A for samples MCM-41, AlMCM-41(a), and AlMCM-41(b).

volume concept. This model takes into account that, first, a reorientation of a molecular dipole is only possible when a sufficiently free local volume V_f exists at the site of the molecule and, second, the free volume determines the efficiency of the reorientation process. Then, the attempt relaxation time will obviously decrease if the molecule has a larger free local volume available for reorientation according to $\tau_0 \propto \exp(c/V_\mathrm{f})$ [32] where c is a numerical factor. We must remember that the surface of the mesoporous aluminosilicates pore walls becomes more hydrophilic with decreasing $n_\mathrm{Si}/n_\mathrm{Al}$ ratio. Consequently, the density of the interfacial water layer rises with the aluminium framework concentration in the samples AlMCM-41(a) and AlMCM-41(b). Thus, the free local volume a water molecule requires for a reorientation decreases, and the attempt relaxation time τ_0 becomes longer in agreement with the experimental values presented in table 2.

The experimentally obtained parameters of the double-well potentials (figure 9) show that their barrier height E_b has a weak temperature dependence, but features the overall trend E_b (MCM-41) $>$ E_b (AlMCM-41-a) $>$ E_b (AlMCM-41-b). Therefore, E_b decreases with rising framework aluminium concentration in the mesoporous materials. This result seems to be somewhat surprising as it is generally accepted that water is more strongly adsorbed on the surface of aluminosilicates with lower $n_\mathrm{Si}/n_\mathrm{Al}$ framework ratios. However, here the barrier height of the double-well potential does not have the meaning of an adsorption energy but is a measure of the strength of the hydrogen bonds between the water molecules forming the interfacial layer. Thus, the barrier height corresponds to the energy which is required to break the hydrogen bonds and to allow a reorientation of the water dipole. According to the observed dependence of E_b on the $n_\mathrm{Si}/n_\mathrm{Al}$ framework ratio we assume that the strength of the hydrogen bonds is weakened by an increasing number of defects in the interfacial water layer. In general, defects must either increase or decrease the barrier height. If the height increases, the mobility of the dipole decreases, which results in a reduced contribution to the dynamics of permittivity. Therefore, we are not able to 'see' it in the dielectric response. If the barrier height decreases, the mobility increases and the contribution to the permittivity dynamics increases also. This

should result in a decrease of the mean relaxation time and a corresponding decrease of the effective barrier height E_b, which is indeed observed in our experiments (figure 9). Such distortions are caused for instance by either water molecules strongly adsorbed on Brønsted acid sites or sodium cations with their solvation shell embedded in the interfacial water layer. Further experiments on AlMCM-41 materials exchanged with different cations and on their corresponding H form are in progress to support our conclusions.

4. Conclusions

From the dielectric spectroscopy of (hydrated) MCM-41 and AlMCM-41 mesoporous materials three dielectric dispersion regions of the confined water have been found. The dielectric dispersion in the low-temperature region is caused by water molecules forming an interfacial layer with the inner surface of the mesoporous support. On the basis of a regularization technique the relaxation time distributions at various temperatures were obtained in a model independent way and can be interpreted in terms of a reorientation of the water molecular dipole moments in a double-well potential. The strength of the hydrogen bonds in the interfacial layer as expressed by the barrier height of the double-well potentials is strongly influenced by the defect concentration at the surface of the mesoporous materials. The higher defect densities found in materials with lower n_{Si}/n_{Al} framework ratios result in weaker hydrogen bonds. The relatively broad distributions of the relaxation times indicate the dipolar glass nature of the interfacial water layer. The determined freezing temperatures of about 21 K are typical for glass transitions in hydrogen-bonded systems.

Acknowledgments

Financial support by Fonds der Chemischen Industrie (MH and AP) and Alexander von Humboldt Stiftung (JB) are gratefully acknowledged.

References

[1] Kresge C T, Leonowicz M E, Roth W J, Vartuli J C and Beck J S 1992 *Nature* **359** 710
[2] Ying J Y, Mehnert C P and Wong M S 1999 *Angew. Chem. Int. Edn Engl.* **38** 56
[3] Beck J S, Vartuli J C, Roth W J, Leonowicz M E, Kresge C T, Schmit K D, Chu C T W, Olson D H, Sheppard E W, McCullen S B, Higgins J B and Schlenker J L 1992 *J. Am. Chem. Soc.* **114** 10834
[4] Mokaya R, Jones W, Luan Z, Alba M D and Klinowski J 1996 *Catal. Lett.* **37** 113
[5] Sayari A, Danumah C and Moudrakowski I L 1995 *Chem. Mater* **7** 813
[6] Ryoo R, Ko C H, Kim J M and Howe R 1996 *Catal. Lett.* **3** 29
[7] Chen L, Klar P J, Heimbrodt W, Brieler F and Fröba M 2000 *Appl. Phys. Lett.* **76** 3531
[8] Besson S, Gacoin T, Ricolleau C, Jacquiod C and Boilot J-P 2002 *Nano Lett.* **2** 409
[9] Leon R, Margolese D, Stucky G and Petroff P M 1995 *Phys. Rev.* B **52** R2285
[10] Tang Y S, Cai S, Jin G, Wang K L, Soyez H M and Dunn B S 1997 *Appl. Phys. Lett.* **71** 2448
[11] Agger J R, Anderson M W, Pemble M E, Terasaki O and Nozue Y 1998 *J. Phys. Chem.* B **102** 3345
[12] Kohiki S, Takad S, Shimizu A and Yamada K 2000 *J. Appl. Phys.* **87** 474
[13] Sliwinska-Bartkowiak M, Dudziak G, Sikorski R, Gras R, Radhakrishnan R and Gubbins K E 2001 *J. Chem. Phys.* **114** 950
[14] Morishige K and Ito M 2002 *J. Chem. Phys.* **117** 8036
[15] Morishige K and Kawano K 1999 *J. Chem. Phys.* **110** 4867
[16] Hansen E W, Stöcker M and Schmidt R 1996 *J. Phys. Chem.* **100** 2195
[17] Kremer F, Huwe A, Schönhals A and Różański S A 2003 *Broad Band Dielectric Spectroscopy* ed F Kremer and A Schönhals (Berlin: Springer) p 171
[18] Wu C-G and Bein T 1994 *Chem. Mater.* **6** 1109
[19] Morishige K and Nobuoka K 1997 *J. Chem. Phys.* **107** 6965

[20] Baker J M, Dore J C and Behrens P 1997 *J. Phys. Chem.* B **101** 6226
[21] Takahara S, Nakano M, Kittaka S, Kuroda Y, Mori T, Hamano H and Yamaguchi T 1999 *J. Phys. Chem.* **103** 5814
[22] Mansour F, Dimeo R M and Peemoeller H 2002 *Phys. Rev.* E **66** 041307
[23] Sliwinska-Bartkowiak M, Dudziak G, Sikorski R, Gras R, Radhakrishnan R and Gubbins K E 2001 *J. Chem. Phys.* **114** 950
[24] Øye G, Axelrod E, Feldman Y, Sjöblom J and Stöcker M 2000 *Colloid Polym. Sci.* **278** 517
[25] Provencher S W 1982 *Comput. Phys. Commun.* **27** 213
[26] Dolinsek J, Acron D, Zalar B, Pirc R, Blinc R and Kind R 1996 *Phys. Rev.* B **54** R6811
[27] Banys J, Lapinskas S, Kajokas A, Matulis A, Klimm C, Völkel G and Klöpperpieper A 2002 *Phys. Rev.* B **66** 144113
[28] Kutnjak Z, Levstik A, Filipic C, Pirc R, Tadic B, Blinc R, Kabelka H, Fuith A and Warhanek H 1991 *J. Phys.: Condens. Matter* **3** 91
[29] Trybula Z, Schmidt V H and Drumheller J H 1991 *Phys. Rev.* B **43** 1287
[30] Ryabov Ya, Gutina A, Arkhipov V and Feldman Yu 2001 *J. Phys. Chem.* B **105** 1845
[31] Chan R K, Davidson D W and Whalley E 1965 *J. Phys. Chem.* **43** 2376
[32] Frunza L, Kosslick H, Frunza S and Schönhhals A 2002 *J. Phys. Chem.* B **106** 9191
[33] Warnock J, Awshalom D D and Shafer M W 1986 *Phys. Rev. Lett.* **57** 1753
[34] Overloop K and Gerven L V 1993 *J. Magn. Reson.* **101** 179